Published in final edited form as:
Exp Eye Res. 2013 August ; 113: 41–48. doi:10.1016/j.exer.2013.05.003.

Evaluation of Multimodal Imaging in Carriers of X-Linked Retinitis Pigmentosa

Jennifer H. Acton[1,2,3], **Jonathan P. Greenberg**[1], **Vivienne C. Greenstein**[1,3], **Marcela Marsiglia**[1,3,4], **Mirela Tabacaru**[1], **R. Theodore Smith**[3], and **Stephen H. Tsang**[1]

[1]Department of Ophthalmology, Columbia University, New York, NY, USA

[2]School of Optometry and Vision Sciences, Cardiff University, Cardiff, Wales, UK

[3]Department of Ophthalmology, New York University, New York, NY, USA

[4]Vitreous Retina Macula Consultants of NY, New York, NY, USA

Abstract

The aim of this study was to investigate visualization of the tapetal-like reflex using current imaging modalities and evaluate SD-OCT changes in known carriers of X-linked retinitis pigmentosa (XLRP); the objective being the development of an optimal protocol for clinicians to identify carriers. Ten XLRP carriers (19 eyes) were examined using color fundus photography, 488 nm reflectance (488-R), near-infrared reflectance (NIR-R), autofluorescence (AF) and spectral-domain optical coherence tomography (SD-OCT) imaging (Spectralis SLO-OCT, Heidelberg). Horizontal line scans through the fovea were acquired in all subjects and in a group of 10 age-similar controls. Peripheral SD-OCT scans (extending to 27.5° eccentricity) were also acquired in both eyes of 7 carriers. MP-1 microperimetery (10-2 pattern; Nidek) was performed in one eye of each carrier. For the XLRP carriers, a tapetal reflex was observed with all imaging modalities in 8 of 19 eyes. It had the same retinal location on color fundus, 488-R and NIR-R imaging but a different location on AF. The tapetal reflex was most easily detected in 488-R images. The horizontal foveal SD-OCT scans were qualitatively normal, but measurements showed significant outer retinal layer thinning in all eyes. Additionally, the 14 eyes with peripheral SD-OCTs demonstrated patchy loss of the inner segment ellipsoid band. Microperimetry exhibited patchy visual sensitivity loss in 9 eyes. Full field ERGs were variable, ranging from normal to severely abnormal rod and cone responses. Our findings suggest that an optimal protocol for identifying carriers of XLRP should include 488-R imaging in a multimodal approach. Peripheral SD-OCT imaging and central retinal layer quantification revealed significant structural abnormalities.

Keywords

X-linked retinitis pigmentosa; tapetal like reflex; spectral domain optical coherence tomograph; scanning laser ophthalmoscope; microperimetry

Corresponding Author: Stephen H. Tsang, Department of Ophthalmology, Columbia University, Edward S. Harkness Eye Inst. 635 W. 165th Street, 5th Floor New York, NY 10032 001-212-342-1189 001-212-305-4987 (Fax) gene.targeting@gmail.com.

1. Introduction

X-linked retinitis pigmentosa (XLRP) accounts for approximately 20% of families with retinitis pigmentosa (Bird, 1975; Fishman, 1978). Early diagnosis of carriers of XLRP and their sons is essential for genetic counseling and to identify patients that may benefit from future experimental therapy (Beltran et al., 2012). Carriers of XLRP typically present with a tapetal-like reflex, in the posterior pole (Figure 1) and sectoral peripheral bone-spicule fundus changes (Fishman et al., 1986). The tapetal reflex is a golden-metallic shine within the perimacular region that resembles the reflection seen in the fundus of animals with a tapetum. Pigment epithelial thinning and pigment migration into the retina have previously been described in XLRP carriers (Bird, 1975), observed as a slightly grey appearance to the retina rather than the orange/red color of the normal fundus.

Past studies have demonstrated a broad range of visual function findings in carriers, ranging from normal function to severe visual deficits. The following have been reported: normal and constricted visual fields using Goldmann kinetic perimetry (Alexander et al., 2003; Andreasson et al., 2003; Banin et al., 2007; Bird, 1975; Fishman et al., 1998; Grover et al., 2000; Jacobson et al., 1997; Wegscheider et al., 2004); patchy rod and cone system sensitivity loss using two-color threshold perimetry (Gieser et al., 1998; Jacobson et al., 1997; Jacobson et al., 1992; Wegscheider et al., 2004), in which rod and cone sensitivity losses were equal (Fishman et al., 1998; Peachey et al., 1988), or rod loss was greater than cone system loss (Jacobson et al., 1997; Wegscheider et al., 2004) abnormal rod and cone responses on full field electroretinography (ERG)(Banin et al., 2007; Fishman et al., 1998; Gieser et al., 1998; Grover et al., 2000; Jacobson et al., 1997; Peachey et al., 1988; Vingolo et al., 2006) and patchy areas of decreased cone response amplitude and/or increased implicit time using the multifocal ERG technique (Vajaranant et al., 2002). Combined spectral domain optical coherence tomography (SD-OCT) and microperimetry, using the OPKO OCT/scanning laser ophthalmoscope (SLO), found normal retinal structure in 3 XLRP carriers and showed abnormal retinal sensitivity associated with tapetal fundus changes (Genead et al., 2010).

Image analysis of the tapetal reflex discerned tiny point-like circular reflexes, 8.5 μm in diameter, of higher reflectance than the adjacent retina, which did not show significant change over time (Cideciyan and Jacobson, 1994). An abnormal radial pattern on fundus autofluorescence imaging was found in some subjects, which had some correspondence with areas of visual field loss (Wegscheider et al., 2004). Evidence of reduced thickness of the neurosensory retina and increased outer layer reflectivity has been noted from OCT imaging (Jacobson et al., 1997; Vingolo et al., 2006).

The purpose of the study was to investigate visualization of the tapetal like reflex using current imaging modalities and evaluate SD-OCT changes in known carriers of XLRP, the objective being the development of an optimal protocol for clinicians to identify carriers.

2. Materials and Methods

2.1 Subjects

The study comprised 10 female obligate carriers of XLRP (mean age 45.5 ± 12.4 years, range 27-60 years) from 7 families. Subjects underwent a complete ophthalmic examination at Columbia University that included BCVA, refraction, slit-lamp examination and dilated fundus examination.

Patients were diagnosed as carriers of XLRP based upon the typical appearance of a tapetal-like reflex within the posterior pole (in any of the imaging modalities), a family history of

XLRP and results of genetic testing (in 5 of 10 patients). A summary of the clinical characteristics of the subjects is given in Table 1. All subjects had clear ocular media, no systemic or neurological disease, no history of ocular surgery and steady foveal fixation, except for two carriers, who had reduced visual acuity in one eye, due to a history of trauma (C5) and strabismic amblyopia (C10).

Four subjects (C1-C4) belonged to one family (Figure 2). The remaining subjects studied were each from different families and consisted of the mothers of affected males (C5-C9) and the daughter of an affected male (C10).

In 5 patients, the *RPGR* coding region was sequenced for disease-causing mutations. The total genomic DNA was extracted from the peripheral blood with the QIAamp DNA Mini Kit (Qiagen, Valencia, California). The extracted genomic DNA was amplified using polymerase chain reaction (PCR) with previously described primer sequences and annealing temperatures (Ruddle et al., 2009). The PCR products were purified (QIAquick PCR Purification Kit, Qiagen, Valencia, California) and sequenced (Tosi et al., 2009; Wang et al., 2009).

On the basis of genotypic analysis, mutations in the *RPGR* gene were found in 5 women from 2 families (C1-5). In one family, 1 obligate carrier (C5) was found to be heterozygous for a two base pair deletion (c.2997_2998delGG) in exon ORF15. In the other family, 4 women (C1-C4) showed a nonsense (stop) mutation on the exon ORF15 of the RPGR gene (c.2812G>T, p.Glu938X). The other participants of this study did not have genetic analysis.

The study and data accumulation adhered to the tenets of the Declaration of Helsinki for research involving human subjects in accordance with HIPAA regulations and the protocol was approved by the Columbia University Medical Center Institutional Review Board for Human Research. Each participant gave informed written consent prior to enrollment in the study. IRB approval was prospective.

2.2 Ocular Imaging

Digital color fundus photographs were obtained in 19 eyes of the 10 carriers. SLO images were acquired in 19 eyes, using the Spectralis HRA+OCT (Heidelberg Engineering, Heidelberg, Germany). 30° and 55° field images were obtained with the automated real-time (ART) mode, using the following modalities: 488 nm reflectance (488-R; “red-free”), near-infrared reflectance (NIR-R; 820 nm), and autofluorescence (AF) imaging (488 nm excitation, detection >500 nm barrier filter). Images were aligned with an automated image registration algorithm written in Matlab (version 7.7.0; The MathWorks, Natick, Massachusetts, USA) (Chen et al., 2008) for qualitative comparison of the visibility and localization of the tapetal reflex among different imaging modalities (Table 1).

Spectralis SD-OCT 30° (9 mm) horizontal line scans centered at the fovea were captured in all eyes. Horizontal peripheral line scans, extending to eccentricities of approximately 27.5° from the fovea were also acquired in 7 of the carriers (14 eyes). Scans were performed using high resolution settings and ART tracking as an average of 100 scans, to give the highest signal to noise ratio (>25 dB). An additional group of 10 age-similar healthy controls, matched for refractive error, were recruited (mean age 45.1 ± 11.7 years, range 27-60 years) and SD-OCT scans were obtained.

SD-OCT images were segmented in one eye of each subject, using a computer-aided, manual segmentation technique (Figure 3) (Hood et al., 2011; Hood et al., 2009). The segmented borders were the following: INL/OPL: the border between the inner nuclear layer (INL) and the outer plexiform layer (OPL); ISe: the inner segment ellipsoid band (Spaide

and Curcio, 2011) (also known as the inner segment/outer segment junction); OS/RPE: border between outer segment (OS) and retinal pigment epithelium (RPE); BM/choroid: the border between Bruch's membrane (BM) and the choroid. Using the locations of these boundaries, we defined 2 retinal layers as shown in Figure 3: Total receptor (REC+), the distance between INL/OPL and BM/choroid and receptor outer segment plus RPE (OS+), the distance between ISe and BM/choroid.

2.3 Electroretinography

In addition, 4 of the carriers had full-field ERG testing (Diagnosys LLC, Lowell, Massachusetts, USA) in both eyes, performed at our institution, according to ISCEV standards (Marmor et al., 2004). The following ERGs were obtained: Dark-adapted 0.01 “rod response”, dark-adapted 3.0 “combined rod-cone response”, light adapted 3.0 “single-flash cone response” and light adapted 3.0 flicker “30 Hz flicker”. A minimum period of 20 min of dark adaptation preceded the recording of the rod-mediated ERG and following 10 min of light adaptation, the cone ERGs were recorded. The ERGs for each stimulus condition were reproducible. Amplitudes and implicit times were compared to age-similar normal values. ERG testing was performed for another 5 carriers at other institutions.

2.4 Microperimetry

All carriers underwent MP-1 microperimetry (Nidek Instruments Inc., Padova, Italy; NAVIS software version 1.7.3.) testing, using the 10-2 pattern. The carriers had recent experience of at least one visual field test. The MP-1 pattern consisted of 68 test locations within 10° of the fovea with a separation of 2° bet ween stimulus locations. Subjects were tested following pupil dilation with 1% tropicamide and after a 15 minute adaptation period to the test background. The non-tested eye was occluded. White test lights (stimulus size Goldmann III, 200 ms in duration) were presented on a 1.27 cd/m^2 white background using a 4-2 threshold strategy. Subjects were asked to maintain fixation on a 2° red cross. Abnormality was defined using total deviation (TD) defects, derived from a previously collected normative database comprising 50 subjects (age range 18-68 yrs), from which prediction limits were calculated using a linear Bayesian model (Acton et al., 2011).

2.5 Analysis

Results of MP-1 testing from one eye of each subject were included in the analysis and the eye was randomly selected, except in subjects C5 and C7, where the eye with the better vision was included. SD-OCT layer thickness values from the same test eye of each XLRP carrier were compared to values acquired in the control subjects.

Three observers ranked images in order of the prominence and visibility of the tapetal reflex. Agreement among observers was calculated using the Fleiss kappa test for multiple observers.

3. Results

All subjects were asymptomatic, except for one subject (C5) who had visual loss due to pigmentary degeneration. The BCVAs of the tested eyes ranged from 20/20 to 20/40 (Table 1).

3.1 Ocular Imaging

In all XLRP carriers, a tapetal reflex was observed as a hyperreflective radial pattern in 488-R and NIR-R images at the posterior pole (Figure 1; Table 1). The tapetal reflex was present with all imaging modalities in 8 of 19 eyes and had the same retinal location on color fundus, 488-R and NIR-R imaging, but on AF, it had a more widespread location and a more

diffuse appearance. The reflex had greatest visibility in 488-R images, in 16 of 19 eyes and in the remaining 3 eyes, the reflex was most prominent in AF imaging. However, in 7 eyes, the reflex was visible with all imaging modalities except for AF, which least frequently showed the reflex. On color fundus photography, the reflex was not present in 5 eyes.

The following summary describes the possible multimodal imaging observations of the tapetal reflex and provides examples of each (shown in Figure 1):

1. Reflex present with all imaging modalities, but more widespread and diffuse in AF mode (e.g. C10).
2. Greater visibility of the reflex in 488-R (e.g. C1 & C3)
3. Greater visibility of the reflex in AF mode (e.g. C9)
4. Reflex visible with all imaging modalities except AF (e.g. C1 & C8)
5. Absence of reflex on CF (e.g. C9)

A ranking system comparing the prominence of the tapetal reflex among the different imaging modalities is shown in Table 1, and where observers disagreed, the mode rank order is presented. Interobserver agreement was strong for all images (kappa = 0.80, 95% CI = 0.73 to 0.87). For CF, NIR-R and 488-R, agreement among observers was strong (CF: kappa = 0.81, 95% CI = 0.66 to 0.96; NIR-R: kappa = 0.86, 95% CI = 0.61 to 1.0; 488-R: kappa = 0.70, 95% CI = 0.48 to 0.91) and for AF, agreement was moderate (kappa = 0.57, 95% CI = 0.43 to 0.72).

Qualitatively, all SD-OCT images in carriers were unremarkable within the central 30° with the exception of one carrier (C5) who showed disruption of the ISe band and patchy RPE atrophy within the central 30°. However, in the 7 subjects (14 eyes) who had peripheral imaging, patchy yet gradual disruption of the ISe band was observed, starting at eccentricities of 17-20° and extending beyond the limit of the image (Figure 4). There were no disruptions of the ISe band in peripheral SD-OCT images of normal subjects.

The position of the tapetal reflex did not correspond to the peripheral ISe band disruptions, or to any other features in SD-OCT images.

3.2 Retinal Thickness Measurements

Thinning of retinal layers was found in all carriers of XLRP (Figure 5). For XLRP carriers, the mean OS+ thickness was 0.051 ± 0.002 mm and was significantly thinner than that of the controls, 0.054 ± 0.003 mm (unpaired t test: $t = -2.95$, $p = 0.009$). The mean REC+ thickness for XLRP carriers was 0.152 ± 0.008 mm and was also significantly thinner than that of the controls, 0.176 ± 0.008 mm ($t = -6.20$, $p < 0.001$).

3.3 Electroretinography

Table 2 summarizes the ERG findings in 4 of the 10 carriers (C5, C6, C9, C10). Three carriers demonstrated cone-rod dysfunction, represented by decreased cone mediated b-wave amplitudes and decreased rod specific b-wave amplitudes. In one carrier (C5) the rod and cone flash responses were not detectable. Additionally, cone flicker implicit time was delayed in all 4 carriers. With the exception of an inter-ocular difference in cone mediated b-wave amplitudes in 2 carriers, the ERG findings were symmetrical between eyes.

3.4 Microperimetry

The test eye from each subject had steady foveal fixation, as assessed by the fixation tracker of the MP-1 (Figure 6). Microperimetry results from the test eye in each carrier in the central

10° ranged from normal to severe loss (Table 3). The group mean global indices were as follows: mean sensitivity (MS) was 15.30 ± 3.95 dB; mean deviation (MD) was −4.09 ± 3.92 dB; pattern standard deviation (PSD) was 2.46 ± 1.71 dB. The mean number of TD defects was 22.70 ± 17.51.

TD defects were present in areas with and without the tapetal reflex on 488-R imaging. One of the 10 carriers (C8) had normal MP-1 visual sensitivity, showing no TD defects. The overall distribution of defects tended to show greater loss in the inferior retina in a patchy pattern (Figure 7).

4. Discussion

Structural and functional imaging techniques were used to examine the eyes of known carriers of XLRP in order to evaluate the appearance of the tapetal-like reflex and assess SD-OCT changes; the aim being the development of an optimal protocol for the identification of carriers.

The tapetal-like reflex on fundus examination is a useful sign in XLRP carriers (Bird, 1975) and was previously found to have an enhanced appearance in infrared imaging (Genead et al., 2010). We noted the presence of the reflex in all eyes for NIR-R and 488-R imaging, with greater visibility in 488-R imaging; observation of the reflex was less frequent in color fundus and AF imaging. Therefore, to reduce the chance of missing a tapetal reflex the 488-R imaging modality would be clinically useful. Although in this study, the tapetal reflex was detected in all carriers by imaging modalities, it should be noted that imaging modalities alone may not detect all carriers.

The differing sensitivity between imaging modalities could be explained by the use of techniques that limit the spectral range of the illuminating source. The yellow-orange appearance of the tapetal reflex is enhanced when imaged by opposite or complementary colors (e.g. blue at 488nm). In our study protocol, 488-R (“red-free”) imaging using the SLO was selected due to better visibility of the tapetal reflex over the “red-free” mode of the fundus camera (green filter), which also provided superior visibility of the reflex over color fundus imaging.

The appearance of the tapetal reflex on multimodal imaging was mostly symmetrical between eyes. However, in 2 carriers, the reflex was subtly visible in an imaging modality (AF or color fundus) in one eye but it was not visible with that modality in the other eye. Additionally, the order of prominence of the reflex between various imaging modalities differed slightly between eyes in some carriers due to minor differences in the extent or brightness of the reflex (Table 1).

We also found structural changes in SD-OCT images, in the form of thinning of the outer retinal layers within the central 30° in all XLRP carriers. Previous qualitative OCT assessments have reported retinal layer thinning in studies consisting of 2 carriers (Jacobson et al., 1997) and 5 carriers (Vingolo et al., 2006), in agreement with our findings, however in another study of 3 carriers, retinal thickness was observed to be normal (Genead et al., 2010). The finding of thinning of the outer retinal layers in XLRP carriers is consistent with reports of retinal thinning in RP (Hood et al., 2009), as well as thinning of the outer nuclear layer found in a canine model of XLRP carriers (Beltran et al., 2009).

SD-OCT imaging of the peripheral retina revealed disruption of the ISe band in both eyes of all carriers who underwent peripheral SD-OCT imaging. Although the severity of the fundus appearances in carrier states of XLRP can vary greatly (Jay, 1985; Klein et al., 1967a; Klein et al., 1967b; Lyon, 1961), the disease is similar to other forms of RP in that peripheral loss

is more significant than central loss. To our knowledge, previous OCT investigations of XLRP carriers did not include imaging of the peripheral retina. Other OCT related observations in past studies include increases in reflectivity of the RPE in carriers of XLRP (Genead et al., 2010; Vingolo et al., 2006); however, this change was not seen in our results, perhaps due to differences in instrumentation and technique.

The variability in structural and functional data between carriers in this study supports the Lyon hypothesis of random inactivation of X-chromosomes (Jay, 1985; Klein et al., 1967a; Klein et al., 1967b; Lyon, 1961). This may also explain the asymmetry in functional results between eyes as well as the fact that the typical tapetal reflex is interspersed between areas of normal appearing background retina. The known variation in the severity of degeneration amongst carriers of similar ages (Bird, 1975) is also associated with the Lyon hypothesis. In our data, there did not appear to be any clinically meaningful relationships with increasing age, but this may be due to the inability to separate the effect of age from that of random X-chromosome inactivation in our limited sample size.

In agreement with previous studies, measures of visual function in XLRP carriers spanned a broad range of results. Our visual field results are similar to past studies reporting patchy loss on Humphrey visual fields (Jacobson et al., 1997; Vajaranant et al., 2002) and microperimetry testing (Genead et al., 2010). However our results did not consistently show a correspondence between visual field loss and abnormal AF pattern, as previously noted (Genead et al., 2010; Wegscheider et al., 2004). This discrepancy could be explained by the difference in instrumentation, since the background adaptation conditions of the MP-1 have a lower luminance level compared to the OPKO microperimeter. The findings in this study suggest that microperimetry may be useful for monitoring XLRP carriers, however these findings are not specific and interpretation is limited, since thresholds may be mediated by a mixed rod-cone system response or by mainly a cone system response (Crossland MD, et al. IOVS 2012;53:ARVO E-Abstract 4822) in a retinal dystrophy that predominantly affects the rods. ERG results were also similar to those of past studies, in which ERG responses ranged from normal to markedly subnormal (Alexander et al., 2003). In addition to the findings presented in the results, recent clinical reports, from other institutions, suggested that ERG findings in carriers C1 to C3 were within normal limits. Carriers C4 and C8 had decreased cone mediated b-wave amplitudes and increased cone flicker implicit times, in addition in C8 rod specific b-wave amplitudes were decreased.

The limitations of our study are its relatively small sample size and the lack of follow-up of subjects over time. In another study, the appearance of the tapetal reflex was found to remain stable over time (Cideciyan and Jacobson, 1994), which might suggest limited value to following the tapetal reflex longitudinally, but the possibility of subtle change visible only on SLO 488-R imaging should not be ignored. Although prognosis of visual function in carriers is thought to be better predicted by peripheral retinal pigmentary changes than by the tapetal reflex (Bird, 1975; Grover et al., 2000), the reflex is pathognomic and therefore clinically useful.

In summary, we found that the tapetal reflex was most evident in 488-R imaging and that SD-OCT findings revealed thinning of the central outer retina and peripheral disruption of the ISe band. Our findings suggest that for identifying carriers of XLRP, an optimal protocol in a multimodal approach should include the following non-invasive and rapid imaging modalities: 488-R, AF, NIR-R and color fundus. Peripheral SD-OCT imaging and central retinal layer quantification are of interest as adjunct evaluations and may prove to be of clinical value. Our data suggest that imaging is sensitive in detecting an abnormality across a range of ages. Although genetic testing is necessary to confirm carrier status, the results of our non-invasive techniques are relevant to prognosis and monitoring of progression in

XLRP carriers and are useful for genetic counseling of family members affected by XLRP. Our protocol may also be useful in future research to investigate early diagnosis in asymptomatic female XLRP family members with normal fundi.

Acknowledgments

The authors wish to thank Dr Donald C. Hood for use of segmentation software in his laboratory at Dept of Psychology, Columbia University, New York. The study was presented in part at the Association for Research in Vision and Ophthalmology (ARVO) conference 2012.

Funding/support: NIH Grants R01-EY02115, R01-EY09076, R01-EY015520, EY018213 and P30EY019007 (Core Support for Vision Research); The New York Community Trust; Research to Prevent Blindness; Foundation Fighting Blindness; Grant TS080017 from the Department of Defense, Washington, DC. Dr Tsang is a Burroughs Wellcome Program in Biomedical Sciences Fellow and is also supported by the Charles E. Culpeper Partnership for Cures 07-CS3, the Crowley Research Fund, Schneeweiss Stem Cell Fund, New York State N09G-302, and Joel Hoffmann Scholarship.

References

Acton JH, Bartlett NS, Greenstein VC. Comparing the Nidek MP-1 and Humphrey Field Analyzer in normal subjects. Optom. Vis. Sci. 2011; 88:1288–1297. [PubMed: 21822159]

Alexander KR, Barnes CS, Fishman GA. ON-pathway dysfunction and timing properties of the flicker ERG in carriers of X-linked retinitis pigmentosa. Invest Ophthalmol Vis Sci. 2003; 44:4017–4025. [PubMed: 12939324]

Andreasson S, Breuer DK, Eksandh L, Ponjavic V, Frennesson C, Hiriyanna S, Filippova E, Yashar BM, Swaroop A. Clinical studies of X-linked retinitis pigmentosa in three Swedish families with newly identified mutations in the RP2 and RPGR-ORF15 genes. Ophthalmic Genet. 2003; 24:215–223. [PubMed: 14566651]

Banin E, Mizrahi-Meissonnier L, Neis R, Silverstein S, Magyar I, Abeliovich D, Roepman R, Berger W, Rosenberg T, Sharon D. A non-ancestral RPGR missense mutation in families with either recessive or semi-dominant X-linked retinitis pigmentosa. Am J Med Genet A. 2007; 143A:1150–1158. [PubMed: 17480003]

Beltran WA, Acland GM, Aguirre GD. Age-dependent disease expression determines remodeling of the retinal mosaic in carriers of RPGR exon ORF15 mutations. Invest Ophthalmol Vis Sci. 2009; 50:3985–3995. [PubMed: 19255154]

Beltran WA, Cideciyan AV, Lewin AS, Iwabe S, Khanna H, Sumaroka A, Chiodo VA, Fajardo DS, Roman AJ, Deng WT, Swider M, Aleman TS, Boye SL, Genini S, Swaroop A, Hauswirth WW, Jacobson SG, Aguirre GD. Gene therapy rescues photoreceptor blindness in dogs and paves the way for treating human X-linked retinitis pigmentosa. Proc Natl Acad Sci U S A. 2012; 109:2132–2137. [PubMed: 22308428]

Bird AC. X-Linked Retinitis Pigmentosa. Br. J. Ophthalmol. 1975; 59:177–199. [PubMed: 1138842]

Chen J, Smith RT, Tian J, Laine AF. A novel registration method for retinal images based on local features. Conf Proc IEEE Eng Med Biol Soc. 2008; 2008:2242–2245. [PubMed: 19163145]

Cideciyan AV, Jacobson SG. Image-Analysis of the Tapetal-Like Reflex in Carriers of X-Linked Retinitis-Pigmentosa. Invest Ophthalmol Vis Sci. 1994; 35:3812–3824. [PubMed: 7928178]

Fishman GA. Retinitis Pigmentosa - Genetic Percentages. Arch. Ophthalmol. 1978; 96:822–826. [PubMed: 655919]

Fishman GA, Grover S, Jacobson SG, Alexander KR, Derlacki DJ, Wu WP, Buraczynska M, Swaroop A. X-linked retinitis pigmentosa in two families with a missense mutation in the RPGR gene and putative change of glycine to valine at codon 60. Ophthalmology. 1998; 105:2286–2296. [PubMed: 9855162]

Fishman GA, Weinberg AB, McMahon TT. X-Linked Recessive Retinitis-Pigmentosa - Clinical Characteristics of Carriers. Arch. Ophthalmol. 1986; 104:1329–1335. [PubMed: 3753283]

Genead MA, Fishman GA, Lindeman M. Structural and functional characteristics in carriers of X-linked retinitis pigmentosa with a tapetal-like reflex. Retina. 2010; 30:1726–1733. [PubMed: 20829740]

Gieser L, Fujita R, Goring HHH, Ott J, Hoffman DR, Cideciyan AV, Birch DG, Jacobson SG, Swaroop A. A novel locus (RP24) for X-linked retinitis pigmentosa maps to Xq26-27. Am. J. Hum. Genet. 1998; 63:1439–1447. [PubMed: 9792872]

Grover S, Fishman GA, Anderson RJ, Lindeman M. A longitudinal study of visual function in carriers of X-linked recessive retinitis pigmentosa. Ophthalmology. 2000; 107:386–396. [PubMed: 10690843]

Hood DC, Cho JS, Raza AS, Dale EA, Wang M. Reliability of a Computer-Aided Manual Procedure for Segmenting Optical Coherence Tomography Scans. Optom. Vis. Sci. 2011; 88:113–123. [PubMed: 21076358]

Hood DC, Lin CE, Lazow MA, Locke KG, Zhang X, Birch DG. Thickness of Receptor and Post-receptor Retinal Layers in Patients with Retinitis Pigmentosa Measured with Frequency-Domain Optical Coherence Tomography. Invest Ophthalmol Vis Sci. 2009; 50:2328–2336. [PubMed: 19011017]

Jacobson SG, Buraczynska M, Milam AH, Chen C, Jarvalainen M, Fujita R, Wu WP, Huang YJ, Cideciyan AV, Swaroop A. Disease expression in X-linked retinitis pigmentosa caused by a putative null mutation in the RPGR gene. Invest Ophthalmol Vis Sci. 1997; 38:1983–1997. [PubMed: 9331262]

Jacobson SG, Roman AJ, Cideciyan AV, Robey MG, Iwata T, Inana G. X-Linked Retinitis-Pigmentosa - Functional Phenotype of an Rp2 Genotype. Invest Ophthalmol Vis Sci. 1992; 33:3481–3492. [PubMed: 1464493]

Jay B. X-linked retinal disorders and the Lyon hypothesis. Trans Ophthalmol Soc U K. 1985; 104(Pt 8):836–844. [PubMed: 3868876]

Klein D, Franceschetti A, Hussels I. [Retinitis pigmentosa tied to sex, theory of Mary Lyon and the problem of linkage of chorioretinal abiotrophies with the blood group Xg]. Arch Julius Klaus Stift Vererbungsforsch Sozialanthropol Rassenhyg. 1967a; 42:84–91. [PubMed: 5633068]

Klein D, Franceschetti A, Hussels I, Race RR, Sanger R. X-linked retinitis pigmentosa and linkage studies with the Xg blood-groups. Lancet. 1967b; 1:974–975. [PubMed: 4164603]

Lyon MF. Gene action in the X-chromosome of the mouse (Mus musculus L.). Nature. 1961; 190:372–373. [PubMed: 13764598]

Marmor MF, Holder GE, Seeliger MW, Yamamoto S. Standard for clinical electroretinography (2004 update). Doc Ophthalmol. 2004; 108:107–114. [PubMed: 15455793]

Peachey NS, Fishman GA, Derlacki DJ, Alexander KR. Rod and Cone Dysfunction in Carriers of X-Linked Retinitis Pigmentosa. Ophthalmology. 1988; 95:677–685. [PubMed: 3174027]

Ruddle JB, Ebenezer ND, Kearns LS, Mulhall LE, Mackey DA, Hardcastle AJ. RPGR ORF15 genotype and clinical variability of retinal degeneration in an Australian population. Br J Ophthalmol. 2009; 93:1151–1154. [PubMed: 19429592]

Spaide RF, Curcio CA. Anatomical correlates to the bands seen in the outer retina by optical coherence tomography: literature review and model. Retina. 2011; 31:1609–1619. [PubMed: 21844839]

Tosi J, Janisch KM, Wang NK, Kasanuki JM, Flynn JT, Lin CS, Tsang SH. Cellular and molecular origin of circumpapillary dysgenesis of the pigment epithelium. Ophthalmology. 2009; 116:971–980. [PubMed: 19410955]

Vajaranant TS, Seiple W, Szlyk JP, Fishman GA. Detection using the multifocal electroretinogram of mosaic retinal dysfunction in carriers of X-linked retinitis pigmentosa. Ophthalmology. 2002; 109:560–568. [PubMed: 11874762]

Vingolo EM, Livani ML, Domanico D, Mendonca RHF, Rispoli E. Optical coherence tomography and electro-oculogram abnormalities in X-linked retinitis pigmentosa. Doc Ophthalmol. 2006; 113:5–10. [PubMed: 16955285]

Wang NK, Fine HF, Chang S, Chou CL, Cella W, Tosi J, Lin CS, Nagasaki T, Tsang SH. Cellular origin of fundus autofluorescence in patients and mice with a defective NR2E3 gene. Br J Ophthalmol. 2009; 93:1234–1240. [PubMed: 19429590]

Wegscheider E, Preising MN, Lorenz B. Fundus autofluorescence in carriers of X-linked recessive retinitis pigmentosa associated with mutations in RPGR, and correlation with electrophysiological and psychophysical data. Graefes Arch Clin Exp Ophthalmol. 2004; 242:501–511. [PubMed: 15173948]

Highlights

- The tapetal-like reflex in XLRP carriers was imaged using current imaging modalities.
- Visibility was optimal in 488 nm reflectance images.
- Central SD-OCT scans showed significant outer retinal layer thinning.
- Peripheral SD-OCT imaging demonstrated patchy loss of the inner segment ellipsoid band.
- Optimal clinical protocol for identifying carriers of XLRP should include 488-R imaging.

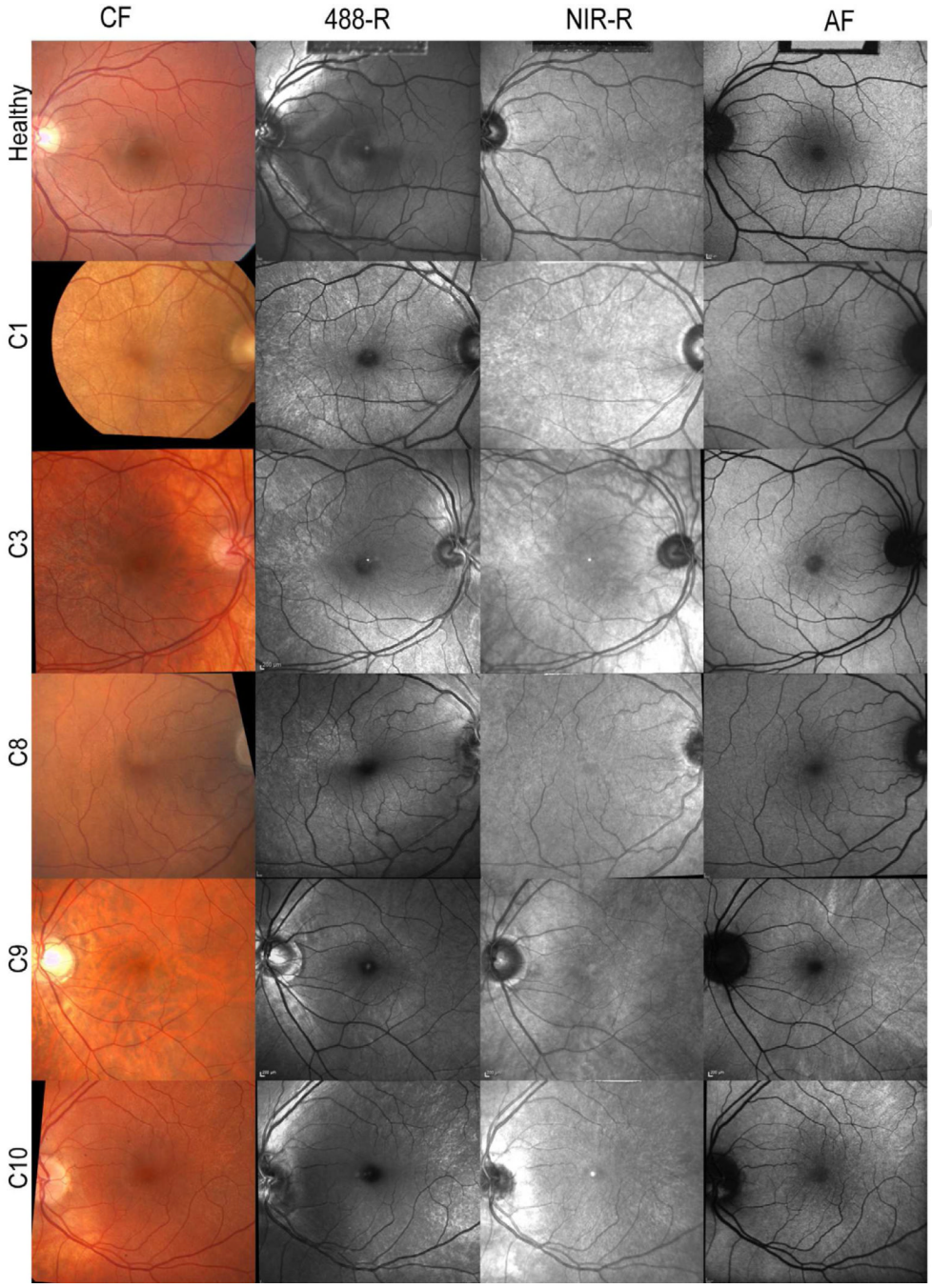

Figure 1.

Color and SLO fundus images of one healthy individual (*top row*) and five XLRP carriers (*from second row to bottom row:* C1,C3, C8, C9, C10)

(*From left to right*) Color fundus (CF), 488 nm reflectance (488-R), near-infrared reflectance (NIR-R) and autofluorescence (AF) images are shown.

The tapetal reflex can be appreciated in the perimacular region as radial lines formed by tiny point-like reflexes which may be elongated in patches or clusters. Where visible, the tapetal reflex has a yellow-orange appearance in CF images (see C1, C3, C8 & C10). In 488-R, NIR-R and AF images, where visible (see Table 1), the tapetal reflex appears bright against the grey fundus background.

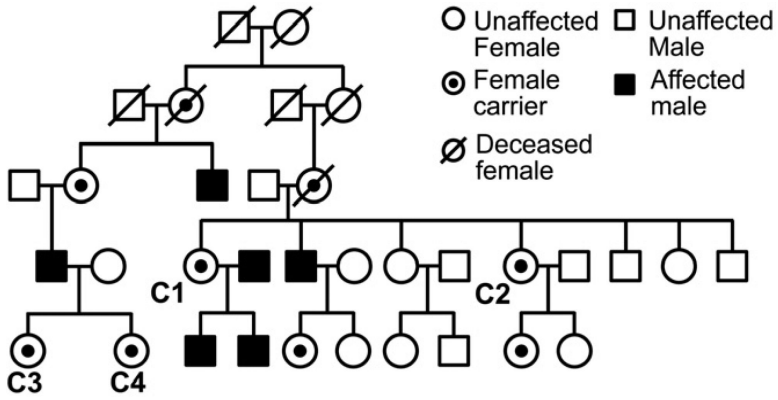

Figure 2.
Pedigree for carriers C1-C4.
The pedigree shows five generations of the XLRP family in this study which includes carriers C1-C4.

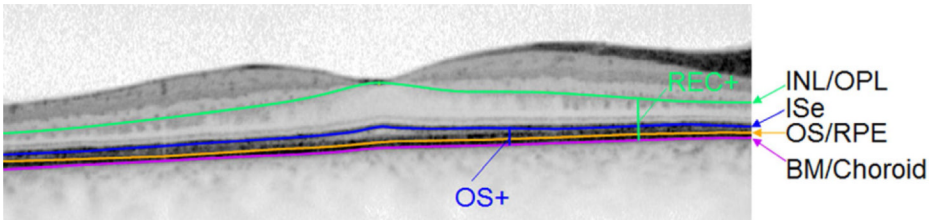

Figure 3.

Segmentation of SD-OCT horizontal scan through the fovea of one XLRP carrier (C8). The layers and bands manually segmented are indicated. INL, inner nuclear layer; OPL, outer plexiform layer; ISe, inner segment ellipsoid band; OS, outer segment; RPE, retinal pigment epithelium; BM, Bruch's membrane; REC+, total receptor; OS+, receptor outer segment plus RPE.

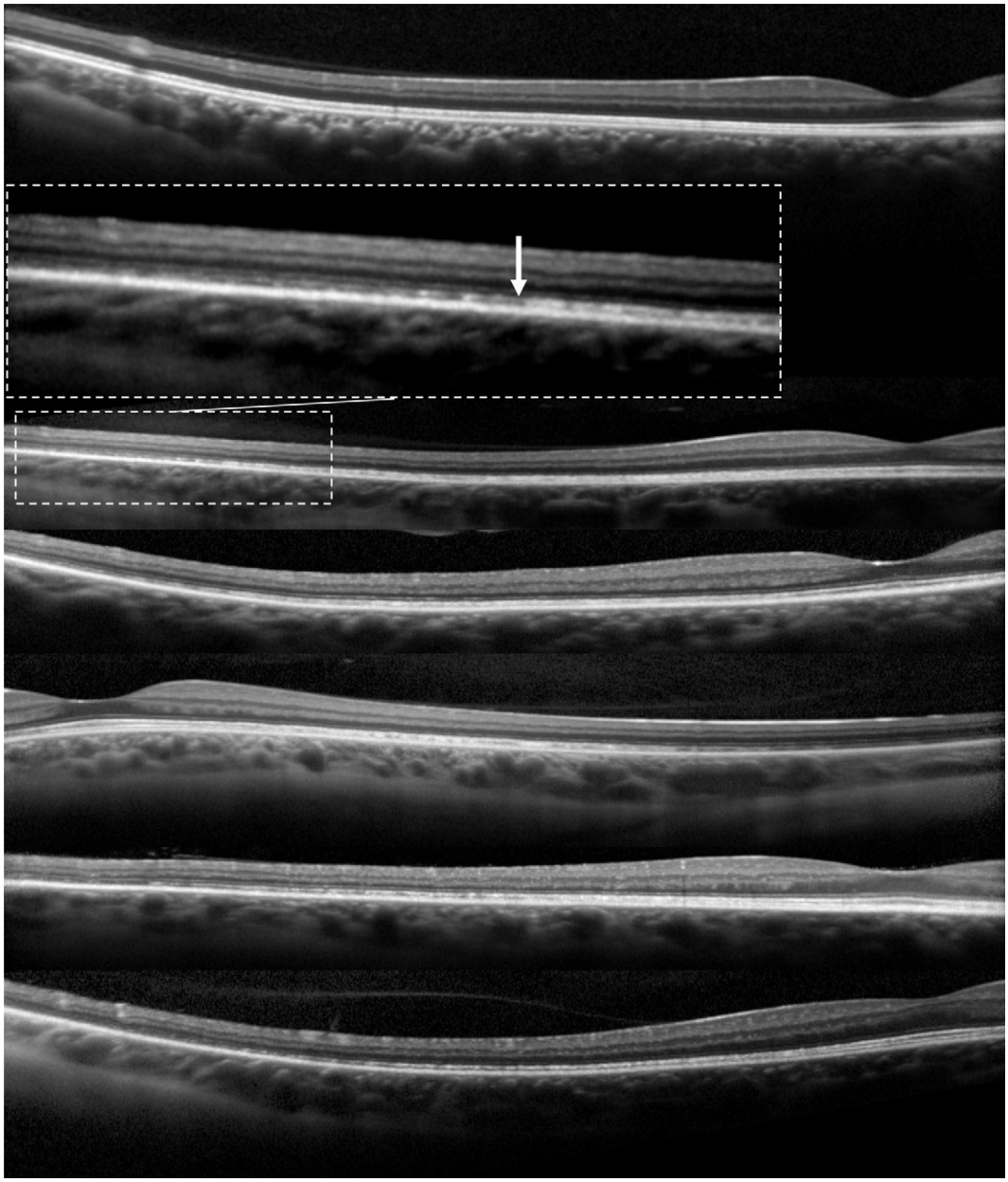

Figure 4.
Peripheral SD-OCT scans.
Peripheral horizontal line scans through the fovea, extending to an eccentricity of 27.5°, of one normal individual (*top*) and five XLRP carriers (*from second row to bottom row:* C10, C1, C3, C8, C9). Enlarged inset image shows peripheral disruption of the ISe (*white arrow*).

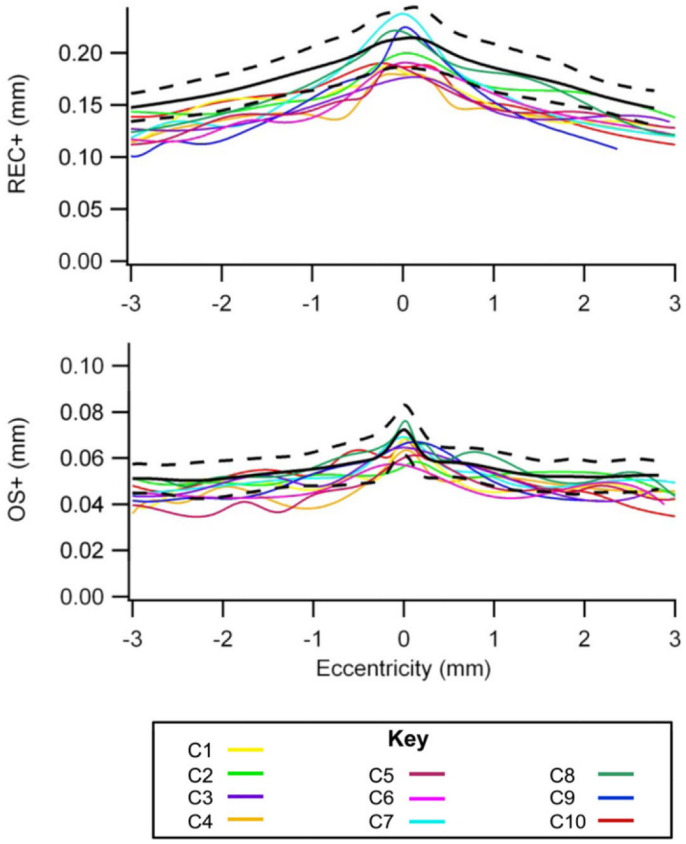

Figure 5.

Retinal layer thickness curves.

Thickness curves for the total receptor (REC+) and the receptor outer segment plus RPE (OS+) layers are shown. All eyes are transposed to a right eye. The colored lines represent each of the XLRP carriers and the black lines are the mean ± 95% confidence intervals for the controls.

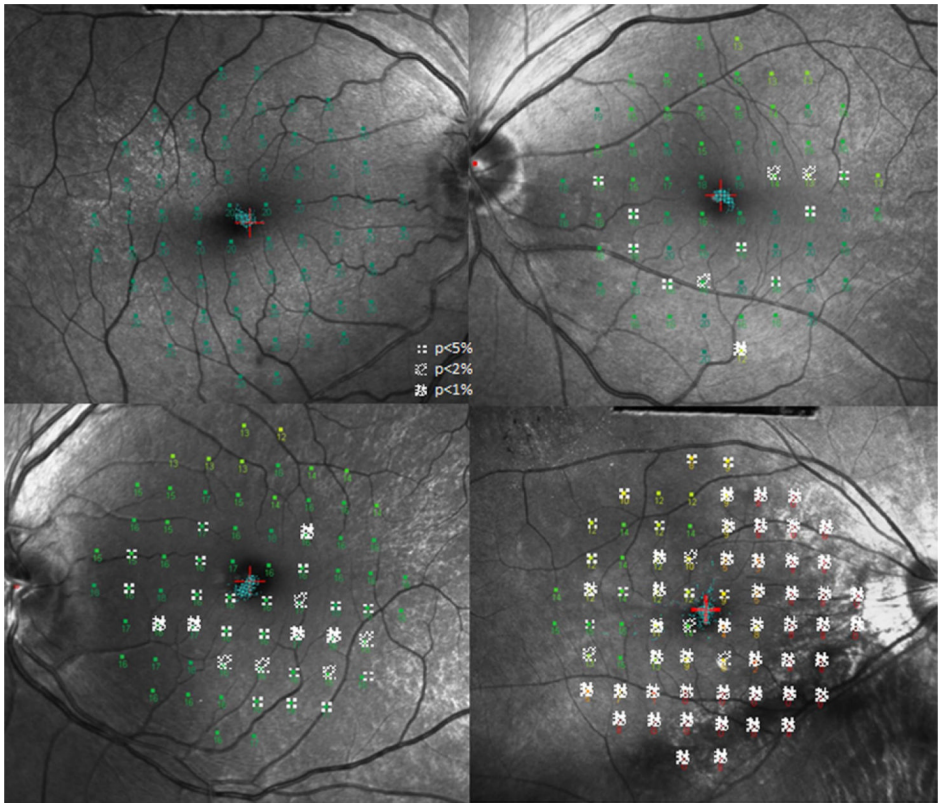

Figure 6.
MP-1 10-2 Total Deviation (TD) probability maps superimposed on 488-R fundus images. Four XLRP carriers (*top left*: C8, *top right:* C7, *bottom left:* C10, *bottom right:* C5) are shown. The TD probability defects show a patchy pattern across the central 10° and visual field sensitivity loss ranges from mild to severe. The fixation pattern is shown in blue around the fixation target (red cross).

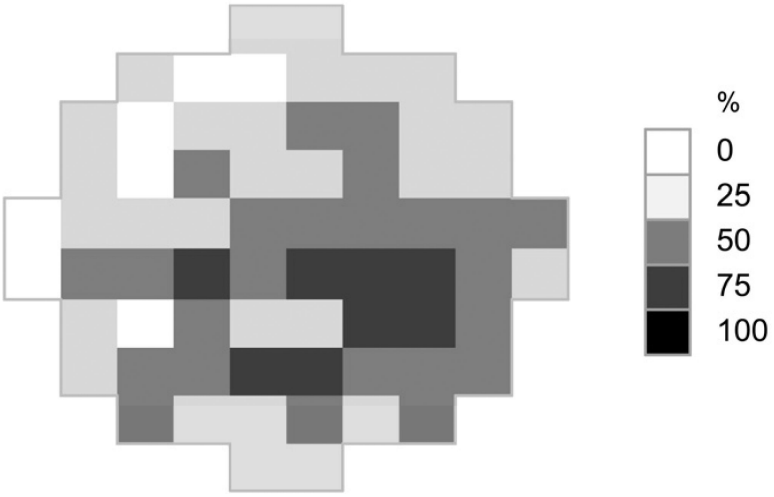

Figure 7.
Frequency of defect map.
The frequency of MP-1 total deviation defects is represented as the percentage of eyes which had a defect of p<5% at each visual field location. All eyes were transposed to a right eye.

Table 1

Clinical characteristics of XLRP carriers.

	Age	Eye	Refraction	VA	Funduscopic appearance	Other
C1	60	OD	+3.25	20/20	tapetal reflex (488-R, NIR-R, CF)	
		OS	+3.25	20/20	tapetal reflex (488-R, NIR-R, CF)	
C2	52	OD	+3.50	20/20	tapetal reflex (488-R, CF, NIR-R)	
		OS	+2.50	20/20	tapetal reflex (488-R, CF, NIR-R)	
C3	32	OD	−6.00	20/20	tapetal reflex (488-R, CF, NIR-R, AF)	
		OS	−6.00	20/20	tapetal reflex (488-R, CF, NIR-R)	
C4	27	OD	Plano	20/20	tapetal reflex (488-R, CF, NIR-R, AF)	
		OS	Plano	20/20	tapetal reflex (488-R, CF, NIR-R, AF)	
C5	60	OD	−3.00	20/25	tapetal reflex (488-R, AF, NIR-R, CF) intraretinal pigment migration	
		OS	−0.50	HM	intraretinal pigment migration, pigmentary degeneration	history of trauma
C6	49	OD	−7.75/−1.00×5	$20/30^{+2}$	tapetal reflex (488-R, NIR-R, AF, CF) peripheral arteriole attenuation	
		OS	−7.75/−1.00×5	$20/30^{+2}$	tapetal reflex (488-R, NIR-R, CF, AF) peripheral arteriole attenuation	
C7	53	OD	−6.50	20/25	tapetal reflex (AF, 488-R, NIR-R) intraretinal pigment migration	
		OS	−6.00	20/40	tapetal reflex (488-R, AF, NIR-R) intraretinal pigment migration	
C8	53	OD	+2.00/−0.25×75	20/20	tapetal reflex (488-R, NIR-R, CF)	
		OS	+3.75/−1.75×50	$20/20^{-1}$	tapetal reflex (488-R, NIR-R)	
C9	38	OD	−0.75/−0.25×45	20/20	tapetal reflex (AF, NIR-R, 488-R)	
		OS	−0.50/−0.25×140	20/20	tapetal reflex (AF, 488-R, NIR-R)	
C10	31	OD	−2.00	20/60	tapetal reflex (488-R, AF, NIR-R, CF)	Strabismic amblyopia
		OS	−2.00	20/20	tapetal reflex (488-R, AF, NIR-R, CF)	

The presence of the tapetal reflex in each imaging modality is indicated by: CF, color fundus; NIR-R, near-infrared reflectance; 488-R, 488 nm reflectance; AF, autofluorescence. Imaging modalities are given in order of most to least prominent tapetal reflex and those that are not mentioned did not did not display the reflex.

Table 2

Full field ERG findings in carriers of XLRP

Carriers		Rod Response	Cone Response		30Hz Flicker
		b-wave amplitude (μV)[a]	**b-wave amplitude (μV)[b]**	**b-wave implicit time (ms)[c]**	**implicit time (ms)[d]**
C5	**OD**	not detectable	not detectable		40
	OS	not detectable	not detectable		37
C6	**OD**	137	68	31	32
	OS	126	64	32	32
C9	OD	145	70	31	26
	OS	149	38	31	26
C10	OD	103	40	31	34
	OS	140	71	30	30

The mean normal values (range) are as follows:

[a] 300 μV (150-450 μV)

[b] 219 μV (101-336 μV)

[c] 30ms (26-34ms)

[d] 26ms (23-28ms)

Table 3

MP-1 results in carriers of XLRP

Carriers		MS	MD	PSD
C1	OS	14.01	−5.29	1.88
C2	OS	14.01	−5.34	2.28
C3	OD	15.66	−3.80	2.83
C4	OS	17.56	−1.92	2.00
C5	OD	5.21	−14.10	7.05
C6	OD	16.94	−2.43	2.21
C7	OS	16.50	−2.85	1.91
C8	OD	20.00	0.65	1.21
C9	OS	17.24	−2.20	2.43
C10	OS	15.82	−3.64	0.83

MS, mean sensitivity (average sensitivity value across the visual field); MD, mean deviation (average sensitivity difference between the measured value and the age-corrected normal value at each stimulus location); PSD, pattern standard deviation (the standard deviation around the mean that constitutes the MD; a measure of variability that is sensitive to localized loss).

The maximum dB value of the MP-1 microperimeter is 20dB. Mean global index values for subjects aged 27-60 years are as follows: MS 18.7 ±0.8 dB; MD −0.8 ± 0.8 dB; PSD 1.3 ± 0.5dB (Acton et al., 2011).